LETTER

Protein-based nanobiosensor for direct detection of hydrogen sulfide

A Letters Journal Exploring the Frontiers of Physics

January 2015

EPL, **109** (2015) 18005 www.epljournal.org
doi: 10.1209/0295-5075/109/18005

Protein-based nanobiosensor for direct detection of hydrogen sulfide

Meisam Omidi[1,3], Ghasem Amoabediny[2,3(a)], Fatemeh Yazdian[1,3] and M. Habibi-Rezaei[4]

[1] *Faculty of New Science and Technology, University of Tehran - Tehran, Iran*
[2] *Department of Biotechnology and Pharmaceutical Engineering, Faculty of Chemical Engineering, School of Engineering, University of Tehran - Tehran, Iran*
[3] *Research Center for New Technologies in Life-Science Engineering, University of Tehran - Tehran, Iran*
[4] *School of Biology, College of Science, University of Tehran - Tehran, Iran*

received 2 September 2014; accepted in final form 19 December 2014
published online 22 January 2015

PACS 87.85.fk – Biosensors
PACS 78.67.Bf – Nanocrystals, nanoparticles, and nanoclusters
PACS 87.14.E- – Proteins

Abstract – The chemically modified cytochrome c from equine heart, EC (232-700-9), was immobilized onto gold nanoparticles in order to develop a specific biosensing system for monitoring hydrogen sulfide down to the micromolar level, by means of a localized surface plasmon resonance spectroscopy. The sensing mechanism is based on the cytochrome-c conformational changes in the presence of H_2S which alter the dielectric properties of the gold nanoparticles and the surface plasmon resonance peak undergoes a redshift. According to the experiments, it is revealed that H_2S can be detected at a concentration of 4.0 μM (1.3 ppb) by the fabricated biosensor. This simple, quantitative and sensitive sensing platform provides a rapid and convenient detection for H_2S at concentrations far below the hazardous limit.

Introduction. – Hydrogen sulfide is a colorless and flammable gas with a "rotten egg" odor. For hundreds of years, it has been recognized as a toxic molecule [1,2]; however, more recent studies suggest that H_2S may also have an important role in cellular signaling pathways [3]. Organisms ranging from bacteria to mammals generate and use H_2S for purposes spanning energy production [4], signal transduction [5], and immune response [6]. With such diverse interest in H_2S, there is a consequent demand for a specific technique for the quantitative measurement of H_2S in both aqueous and gaseous media. Currently available technologies to monitor H_2S levels are based among others on chromatographic [7], spectrophotometric [8], polarographic [9], surface plasmon resonance (SPR) [10,11], amperometric [12], and potentiometric [13] techniques. While each technique has its own advantages [14,15] there remains a need for simple to implement, cheap H_2S sensors that can be used repeatedly [16].

Recently, noble-metal nanoparticles such as gold nanoparticles (GNPs) have received considerable attention in the sensor application because of their SPR shifts under different conditions [17]. Strong variations in SPR are generally observed when these plasmonic nanostructures aggregate as a result of the organic reaction between the coated molecules and analytes. For instance, Zhang *et al.* reported a novel colorimetric probe for the detection of S_2^- and cysteine using simple citrate-stabilized core-shell Cu/GNPs through the S_2^-/cysteine-induced transformation of original and spherical clusters of large, single, spherical particles [18]. Recently fluorescent, DNA-templated Au/Ag nanocluster probes were used for the detection of S_2^- in a turn-off manner [19]. Very recently, Chen *et al.* [20] developed the LSPR sensor for the detection of H_2S with silver nanoparticles. These nanosensors require organic reactions, purification, and surface modification on the particle surface and may encounter difficulties under certain conditions such as different *p*H values. On the other hand, although these methods may provide greater affordability and portability to analytes detection, few of them can be applied to complex environmental matrices. In addition, selectivity is still a problem, so a more robust plasmonic sensor needs to be developed for technological and practical interest.

(a) E-mail: amoabdiny@ut.ac.ir

In order to develop biocompatible, effective and selective devices, biosensors could provide a useful option. The proteins or enzymes, are ideal recognition elements for gases such as NO and H_2S. Electrochemical based biosensors have been widely used for sulfide detection [21–24]. For instance, an amperometric biosensor for sulfide detection in the range 0.5–12.7 μM, with a detection limit of 0.3 μM based on horseradish peroxidase inhibition was reported by Yang *et al.* [22] and Liu *et al.* [23]. The sulfide inhibitory amperometric biosensor based on *Coprinus cinereus* peroxidase with linear response in the range 1.09–16.3 μM, (detection limit of 0.3 μM) and a response time of 43 s was developed by Shahidi Pour Savizi *et al.* [24]. Although the detection limit in these amperometric biosensors was improved, the poor selectivity still remains a main problem, which has restricted its applicability. An optical biosensor for sulfide detection based on fungal peroxidase was developed by Kariminia *et al.* [25]. Strianese *et al.* proposed myoglobin (Mb) and cobalt peptide deformylase (Co-PDF) as a H_2S sensor by means of a fluorescence resonance energy transfer (FRET) mechanism [26,27]. Although these probes can detect H_2S in aqueous solution with high selectivity, usually these biosensors suffer from the low amplitude of the fluorescence signals. In order for metalloproteins to be effectively used as optical biosensors, their sensitivity needs to be increased and the limits of detection (LOD) need to be reduced.

Cytochrome c (cyt c) is a globular water-soluble heme protein with 12.4 kDa molecular weight that exists in the space between the inner and the outer membranes of mitochondria. It plays an important role in the biological respiratory chain, whose function is to receive electrons from cyt-c reductase and deliver them to cyt-c oxidase [28]. In the protein structure of cyt c, the heme group is located in a hydrophobic pocket, in this kind of protein structure, hydrogen sulfide, nitric oxide and carbon monoxide may bind to the heme iron in a reduced form, and only hydrogen sulfide and nitric oxide can bind to the oxidized state of heme iron [29,30]. Consequently, the cyt c in the oxidized form can be employed as ideal recognition element in biosensor for selective H_2S detection.

In this study, we sought to create sensitive proteins/GNPs optical transducers for H_2S detection. We developed a new approach for attaching cyt c onto GNPs which is based on the chemical introduction of thiol derivatives to cyt c. The cyt c/GNPs probes are prepared by introducing GNPs into the solution of chemically modified cyt c. This probe operated on a basic principle; when H_2S reacts with the protein's heme center, cyt c will undergo conformational changes. These changes in the structure of protein affect the dielectric properties of GNPs. These conformational changes were studied by UV-visible, and circular-dichroism (CD) spectroscopic techniques. We have also demonstrated that the system efficiently works as optical H_2S sensor.

Materials and methods. –

Chemicals and materials. Horse heart cytochrome c (EC 232-700-9), 3-mercaptopropionic acid (MPA), N-(3-dimethylaminopropyl)-N′-ethylcarbodiimide hydrochloride (EDC), N-hydroxysuccinimide (NHS), sodium citrate dehydrate, ascorbic acid and phosphate buffer solution (PBS), were all purchased from Sigma-Aldrich. Hydrogen tetrachloro aurate (III) (HAuCl4 • 3H2O) was from Alfa Aesar and the other reagents were purchased from Merck.

Synthesis of GNPs. In a typical synthesis route, GNPs were synthesized with diameters in the range 12–48 nm through sodium citrate reduction of hydrogen tetrachloro aurate (III). In brief, 100 mL of 0.3 mM $HAuCl_4 \bullet 3H_2O$ was brought to a vigorous boil with stirring; subsequently, 1.0 mL of 5 mM sodium citrate was added rapidly to the solution. The solution was boiled for another 10 min, during which the solution color was changed from pale yellow to deep red. The solution was allowed to cool down to room temperature with continued stirring, and then stored in a refrigerator until further use [31].

Preparation of modified cyt c. The horse heart derived chemically modified cyt c when the carboxyl group of 3-mercaptopropionic acid reacted with lysine residues of cyt c via 1-[3-(dimethylamino)propyl]-3-ethylcarbodiimide/N-hydroxysuccinimide (EDC/NHS) activation [32]. As a typical prescription, 87 μL MPA, 0.16 g EDC and 0.12 g NHS were added to 10 mL PBS (*p*H 7.0) under vigorous stirring. Then, 10 μL of this solution were added into the 0.1 mL of 100 μM cyt c in PBS (*p*H 7.0) followed by a gentle stirring at room temperature for 2 h. The protein in the final mixture was reduced by the addition of ascorbic acid and then excess reagents were removed by a separation column. The concentration of cyt c in mixture was estimated by absorption measurements; stock solutions were stored at 4 °C.

GNP conjugation with cyt c. The modified MPA cyt c was incubated with GNPs for 1 h. The resultant mixture was centrifuged to discard the free cyt c and washed by PBS. The target cyt c/GNPs bioconjugates were finally dispersed under ultrasonication in PBS (*p*H 7).

H_2S calibration solution. According to the literature procedure [33], a saturated solution of H_2S with an approximate concentration of 12 mM at 20 °C was prepared by bubbling H_2S gas in 5 ml of PBS (*p*H 7) for 1 h. Also standard solutions of $(NH_4)_2S$ were prepared by a 40% (v/v) commercial solution of $(NH_4)_2S$. The Coulombometric titration was used for determination of the H_2S content of each solution. To avoid the dispersion of H_2S, all the measurements with gas were performed in a sealed cell.

Instrumentation. The morphology of the samples was observed using a JEM 2010 HT transmission electron microscope (TEM) at 200 kV. The absorption spectra

were recorded on a TU-1810 UV-vis-NIR spectrophotometer and circular dichroic (CD) spectra were measured with a Chirascan circular-dichroism spectrometer (Applied Photophysics). Particle size and size distribution were determined by a BI-200SM dynamic light scattering instrument (DLS; Brookhaven Instruments). The value of the ζ potential of the prepared GNPs, cyt c, and cyt c/GNPs bioconjugates were measured with a Zeta potential analyzer (Nano Z, Malvern).

Results and discussion. –

Characterization of GNPs and the cyt c/GNPs bioconjugates. The GNPs with various sizes showed a color from reddish-purple (4 nm) to dark red (40 nm) owing to the collective oscillation of electrons in the conduction band known as LSPR [31]. The shape and size of the synthesized GNPs were characterized by TEM (fig. 1(a)). The prepared GNPs are almost spherical with a diameter of about 23 nm. The TEM results also show that the prepared GNPs are well dispersed. Consequently, the high surface area of the GNPs is available for the assembly of proteins that is an important feature for the GNPs being used as a substrate to fabricate protein/GNPs bioconjugates. The DLS results for the GNPs are shown in fig. 1(b). The DLS measurement demonstrated the narrow size distribution of the prepared nanoparticles. The average hydrodynamic diameters of the GNPs that are obtained from DLS analysis are about 21 nm, which is in good agreement with the values obtained from the TEM results. Usually, the chemical treatment of GNPs in the classical approach leads to the partial aggregation. In the classical chemical treatment, NHS esterification of the carboxyl group on the GNPs surface can destroy the carboxyl ionization. Thus, the negative charge of nanoparticle neutralized which can result in colloidal particle aggregation [21]. However, by using the present approach mentioned above, a dramatic decrease was observed in the particle aggregation.

Presuming that all $AuCl^{-4}$ ions in the solution can be reduced in each preparation, the concentration of the prepared GNPs can be calculated [31]. The concentration of GNPs calculates about 10 nM, from the average volume of a GNP together with this assumption.

The diameter of GNPs has a significant increase after the assembly of cyt c. The average diameter of GNPs changed from 21 nm to about 27 nm which can show the formation of the cyt c/GNPs bioconjugate. Moreover, the shape and size of the cyt c/GNPs were also examined by TEM (fig. 1(c)). It is clear that the cyt c/GNPs keeps its spherical shape and the average diameters obtained from TEM are about 29 nm, which is in good agreement with these values obtained from the DLS results. Furthermore, DLS analysis was also used to measure the size of cyt-c molecules and to evaluate the aggregate degree of the molecules in solution. DLS results indicated that the size of cyt c in solution is 3.1 ± 0.6 nm, suggesting that cyt-c molecules do not undergo significant aggregation

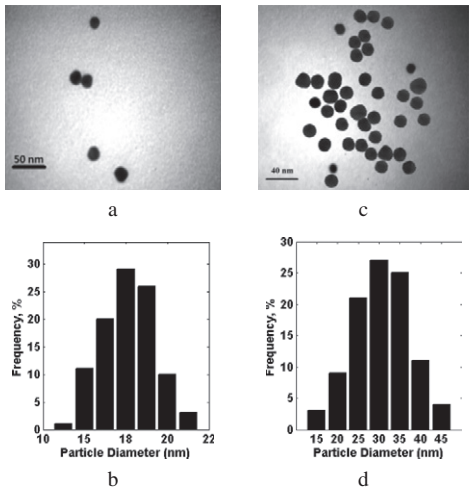

Fig. 1: (a) TEM image and (b) DLS size distribution of GNPs; (c) TEM image and (d) DLS size distribution of cyt c/GNPs.

because cyt c in its native state is approximately spherical in shape [28].

The ζ potential measurements can also confirm the formation of the cyt c/GNPs bioconjugates. The electrical potential at the surface of the bioconjugates which is related to the surface charge and the thickness of the double layer is represented by the ζ potential value. So the ζ potential depends on the amount of proteins assembled at the bioconjugates surface.

The GNPs with the size of 21 nm present a ζ potential of -39 ± 1.6 mV and after the assembly of cyt c the ζ potential by a 14 mV positive shift increases to -25 ± 1.4 mV, which suggests the formation of the cyt c/GNPs bioconjugates. Moreover, these values agree well with previous reports on citrate-stabilized GNPs [34].

Figure 2(a) shows the absorption spectra of the GNPs (black curve) and cyt c/GNPs (red curve). The GNPs have a LSPR peak at $\sim$520 nm. The absorption spectrum of cyt c/GNPs exhibits a LSPR absorption band at $\sim$525 nm ($\sim$5 nm redshift) and a low-intensity protein's Soret band at $\sim$410 nm. This redshift in the LSPR peak is related to the changes in the dielectric constant of the neighboring environment [19]. Moreover, the extinction cross-section of the LSPR of the cyt c/GNPs decreases by about 3% compared to GNPs. Furthermore, the absorption intensity of the Soret band at 410 nm of cyt c was used for calculating the number of cyt-c molecules per nanoparticle. It was found that a self-assembled monolayer of cyt-c molecules was present around the GNPs ($\sim$130 cyt-c molecules per GNPs).

To verify the presented experimental results, they are compared with the Mie theory model [35]. The Mie theory can be used for the simulation of the optical property of core/shell nanoparticles [36]. Up to now, a large number of computer codes of the Mie theory have been developed [37]. Here, we use Mielab [38], a free software specially designed for computing optical properties of multilayered spheres. The theory basis of Mielab is

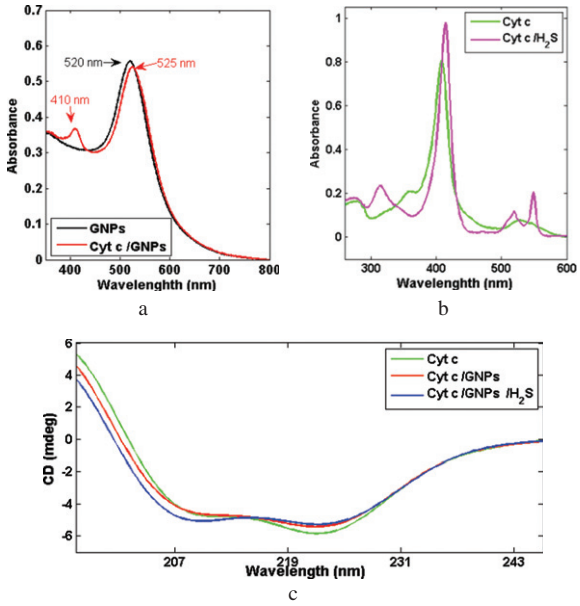

Fig. 2: (Color online) (a) Absorption spectra of GNPs and cyt c/GNPs. Protein concentration: 140 nM in 100 mM PBS (pH = 7). (b) Absorption spectra of free cyt c and cyt c/H_2S-bound in PBS (pH = 7). (c) CD spectra of the free cyt c, cyt c/GNPs and cyt c/GNPs /H_2S-bound.

illustrated by Yang [39]. In the case of the alone GNPs core (AD_p = 20 nm) in water (refractive index = 1.33) the simulation results show an absorption peak at 525 nm, and for the monolayer of the cyt c of 3 nm thickness (size of cyt c in solution) on the GNPs core the simulation results show an absorption peak at 531 nm. It is clear that the simulation results of the Mie theory and the experimental results agree well and this agreement proves the presented experimental results. It is important to note that in the simulation the cyt-c complex refractive index was determined by Yeung *et al.* [40].

Interaction of cyt c with H_2S. The H_2S-induced conformational change of cyt c was studied with UV-vis absorption spectroscopy. Figure 2(b) shows comparative absorption spectra of the H_2S-free (black curve) and H_2S-bound (red curve) spectra. The cyt c has several absorption peaks at 280 nm (Trp absorption peak), at 350 nm (ε-band), at 410 nm (Soret band) and at 533 nm (Q-band) [28]. When H_2S was bubbled through a cyt-c solution, the absorption spectrum significantly changed emphasizing on; the Soret band that revealed redshift and extensive hyperchromocity in the 530 region was bifurcated due to H_2S binding. The ε-band is blueshifted in comparison with its H_2S-free value (H_2S-bound 314 nm; H_2S-free 350 nm, respectively). There is also a decrease in the Trp band. So the change in absorbance in all bands indicates that H_2S can impact the absorption behavior of the protoporphyrin IX double-band resonance, iron coordination and also the structure of the cyt c. The change in the Soret band and the Q-band reflects the changes of the heme micro-environment for the cyt c/H_2S-bound.

Circular-dichroism (CD) spectroscopic measurements were also performed as the most powerful methods to evaluate the extent of the conformational changes of cyt c in the bioconjugate system in comparison to the native protein. Figure 2(c) exhibits the far-UV CD spectra for free cyt c (blue curve), cyt c/GNPs (red curve), and cyt c/GNPs/H_2S-bound (black curve). It is known that when the polypeptide chain exists in the α-helical conformation, there are two native minima at ∼209 and ∼222 nm and a positive band at ∼190 nm. On the other hand, the positive and negative band appeared at 190 and 222 nm, respectively, because of the existence of a β-sheet. CD spectra exhibited two negative minima at 209 and 222 nm that are characteristic of cyt-c high α-helix content. The CD spectrum of cyt c/GNPs/H_2S-bound exhibits a significant alteration on the cyt-c secondary structure. The UV-vis and CD absorption data indicate that the protein undergoes a strong structural change when H_2S binds to cyt c.

Determination of the binding affinity constant. To determine the binding affinity of cyt c for H_2S, H_2S titrations of free cyt c were performed while monitoring the absorption intensity of the Q-band. The relation between the observed absorption intensity, A_H, and K_d is given by [41]:

$$A_H = A_0 - \left(\frac{A_0 - A_\infty}{[\mathrm{H_2S}] + K_d} [\mathrm{H_2S}] \right), \qquad (1)$$

where $[H_2S]$ is the concentration of free H_2S in solution and A_0 and A_∞ denote the absorption intensities of the H_2S-free and H_2S-bound protein, respectively. According to eq. (1) K_d is independent of the labeling ratio. Since the protein concentrations used in the experiments were small compared to the H_2S concentrations, for practical purposes the free $[H_2S]$ could be set equal to the total amount of added H_2S and the data points in fig. 3(a) could be directly fitted to eq. (1) resulting in a K_d of 3.4±0.1 μM for the cyt c.

Sensing mechanism and sensitivity. The magnitude of the spectral shift of LSPR extinction, or the maximum scattering wavelength for small GNPs is described by the following relationship [17]:

$$\Delta\lambda_{\mathrm{LSPR}} = m\Delta k \left(1 - \exp\left(\frac{-2d}{l_d} \right) \right), \qquad (2)$$

where m is the bulk refractive index response of the GNPs, also known as the sensitivity factor (in nm per refractive index unit, RIU), Δk is the change in refractive index (in RIU), d is the effective thickness of the adsorbed layer (in nm) and l_d is the characteristic EM field decay length (in nm). The calculation of the shift of the LSPR extinction for the coated GNPs requires information about the dielectric constants of the cyt-c layer. According to eq. (2), both the attachment of cyt c on GNPs and the conformational change of the protein attached on GNPs are expected to affect the LSPR wavelength (λ_{LSPR}). A change

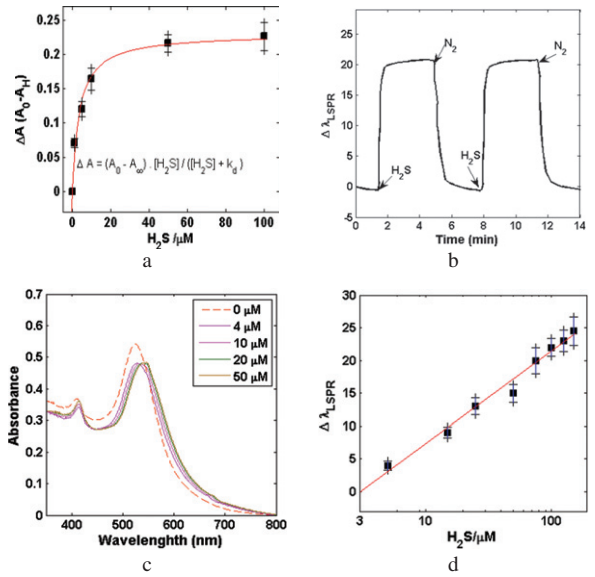

Fig. 3: (Color online) (a) Titration of free cyt c with H_2S monitored by the Q-band absorption intensity (533 nm). The solid line represents the best fit to the data (eq. (1)) with $K_d = 3.4 \pm 0.1$. (b) Room temperature redshifted wavelength of LSPR peak ($\Delta\lambda_{\mathrm{LSPR}}$) time trace observed, upon addition and removal 100 μM of H_2S. (c) Absorption spectra of cyt c/GNPs in the presence of different concentrations of H_2S. (d) Redshifted wavelength of the LSPR peak ($\Delta\lambda_{\mathrm{LSPR}}$) as a function of H_2S concentration. Protein concentration: 140 nM in 100 mM PBS (pH = 7).

in $\Delta\lambda_{\mathrm{LSPR}}$ is employed to quantitatively determine the amount of H_2S. Figure 3(b) shows a typical time trace of the redshifted wavelength of the LSPR peak ($\Delta\lambda_{\mathrm{LSPR}}$). In this particular experiment each cycle was started by adding H_2S to an end concentration of 100 μM and completed by passing nitrogen through the solution for the complete removal of H_2S. A $\Delta\lambda_{\mathrm{LSPR}}$ of cyt c/GNPs clearly undergoes redshifts upon each H_2S addition. When bubbling nitrogen through the sample solution to displace the H_2S, the initial wavelength of LSPR peak was restored; the cycle could be repeated many times. This finding showed that, in the experimental conditions tested, the H_2S binding process is reversible, which is crucial for practical sensing applications. As shown in fig. 3(c), as the amount of H_2S in the aqueous solution is increased, the LSPR wavelength (λ_{LSPR}) of the cyt c/GNPs undergoes redshifts continuously. Furthermore, a linear relationship between $\Delta\lambda_{\mathrm{LSPR}}$ and the H_2S concentration can be inferred (fig. 3(d)), indicating a dynamic range from 0 to 150 μM. The detection limit, defined here as the lowest concentration of analytes in the sensitivity regime, is 4 μM (1.3 ppb). This performance compares favorably with many other spectroscopic or electrochemical methods, suggesting that the cyt c/GNPs constitute a highly sensitive radiometric sensor and $\Delta\lambda_{\mathrm{LSPR}}$ can be used to quantitatively determine the H_2S concentration in an aqueous solution.

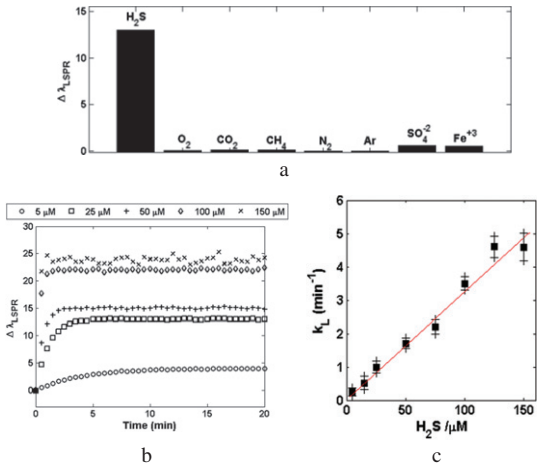

Fig. 4: (Color online) (a) Redshifted wavelength of the LSPR peak ($\Delta\lambda_{\mathrm{LSPR}}$) in the presence of various anions and gases in the same concentration of 20.0 μM. (b) Redshifted wavelength of the LSPR peak ($\Delta\lambda_{\mathrm{LSPR}}$) time traces of cyt c/GNPs after the addition of H_2S. (c) The values of k_L have been plotted as a function of the H_2S concentration. Protein concentration: 140 nM in 100 mM PBS (pH = 7). All time traces were measured at room temperature.

Selectivity. The selectivity is known as a key parameter in nanobiosensors. In order to investigate the selectivity of the present nanobiosensor, the influence of various gases (CH_4, N_2, O_2, Ar and CO_2) and ions (Fe^{3+} and SO_4^{-2}) was tested (fig. 4(a)). The results indicated that in a constant response time, no significant shift is observed in samples containing other anions or gases included. The results demonstrate that the cyt c/GNPs have a high selectivity for the sensing of H_2S in aqueous solutions.

Determination of H_2S binding kinetics. Figure 4(b) shows the spectral shift of LSPR as a function of time after adding various amounts of H_2S in the range 5–150 μM. The spectral shift of LSPR time traces could be well fitted to an exponential function,

$$\Delta\lambda_{\mathrm{LSPR}} = \left\{\lambda_{(t\to\infty)} - \lambda_0\right\}\left(1 - \exp(-k_L t)\right). \qquad (3)$$

When plotting the k_L values as a function of the H_2S concentration, a linear dependence was observed. The k_L can be described by the following relationship:

$$k_L = k_{\mathrm{off}} + k_{\mathrm{on}}[\mathrm{H_2S}], \qquad (4)$$

where k_{off} is the rate of dissociation of the H_2S from the c GNPs/Cyt/H_2S complex and k_{on} is the second-order rate constant for the association of H_2S and cyt; the following values could be extracted from the data in fig. 4(c): $k_{\mathrm{off}} = 0.101 \pm 0.003\,\mathrm{min}^{-1}$, and $k_{\mathrm{on}} = 0.033 \pm 0.001\,\mu\mathrm{M}^{-1}\,\mathrm{min}^{-1}$. From these a value of $K_d = k_{\mathrm{off}}/k_{\mathrm{on}} = 3.1 \pm 0.8\,\mu$M is found in agreement with the K_d values derived from the H_2S titrations (see above). K_d is the key parameter for determining the sensitivity of the sensor. K_d is defined as [cyt c] [H_2S]/[cyt c − H_2S], where [cyt c] is the concentration of the H_2S-free and [cyt c − H_2S] the

concentration of the H_2S-bound cyt c. The quantity by which the sensitivity of the method can be judged is the ratio [cyt c]/[cyt c − H_2S]. This ratio varies strongly when the [H_2S] is close to the K_d. Therefore, with the present nanobiosensor, H_2S can be easily detected in the concentration range between 4 μM and 150 μM.

In order to study the effect of the time stability, the detection of 10 μM H_2S in different time was tested. According to the experimental results it is clear that after 2 months (at 4 °C) the sensor response changes by just about 10 percent. Additional experiments show that the nanobiosensors are stable in the aqueous solution for at least 10 days at room temperature (∼25 °C) before particle sedimentation occurs, regardless of whether H_2S is present or not.

Conclusions. – The Au/cyt c core/shell NPs can be successfully used as a LSPR-based nanobiosensor for H_2S. The cyt c/GNPs probes are prepared by introducing GNPs into the solution of chemically modified cyt c. UV-visible absorption spectroscopy and the circular-dichroism (CD) technique demonstrated that the conformation of cyt c can be changed in the presence of H_2S. This conformational change altered the dielectric properties of the GNPs and induced redshifts in the LSPR band. The H_2S can be easily detected by the present nanobiosensor in the range from 4 μM to 150 μM. In addition to the high sensitivity and selectivity, the sensor also showed a good stability. This simple, rapid, selective, and highly sensitive assay has potential applications in environmental inspection and biomedical research.

REFERENCES

[1] Reiffenstein R. J., Hulbert W. C. and Roth S. H., *Annu. Rev. Pharmacol. Toxicol.*, **32** (1992) 109.
[2] Hendrickson R. G., Chang A. and Hamilton R. J., *Am. J. Ind. Med.*, **45** (2004) 346.
[3] Kamoun P., *Amino Acids*, **26** (2004) 243.
[4] Fu M. *et al.*, *Proc. Natl. Acad. Sci. U.S.A.*, **109** (2012) 2943.
[5] Li L., Rose P. and Moore P. K., *Annu. Rev. Pharmacol. Toxicol.*, **51** (2011) 169.
[6] Shatalin K., Shatalina E., Mironov A. and Nudler E., *Science*, **334** (2011) 986.
[7] Howard A. G. and Yeh C. Y., *Anal. Chem.*, **7** (1998) 4868.
[8] Guenther E. A., Johnson K. S. and Coale K. H., *Anal. Chem.*, **73** (2001) 3481.
[9] Canterford D. R., *Anal. Chem.*, **47** (1975) 88.
[10] Tabassum R., Mishra S. K. and Gupta B. D., *Phys. Chem. Chem. Phys.*, **15** (2013) 11868.
[11] Mishra S. K., Rani S. and Gupta B. D., *Sens. Actuators B: Chem.*, **195** (2014) 215.
[12] Lawrence N. S., Jiang L., Jones T. G. J. and Compton R. G., *Anal. Chem.*, **75** (2003) 2499.
[13] Hassan S. S. M., Marzouk S. A. M. and Sayour H. E. M., *Anal. Chem. Acta.*, **466** (2002) 47.
[14] Nagano T. and Yoshimura T., *Chem. Rev.*, **102** (2002) 1235.
[15] Lim M. H. and Lippard S. J., *Acc. Chem. Res.*, **40** (2007) 41.
[16] Franz K. J., Singh N., Spingler B. and Lippard S. J., *Inorg. Chem.*, **39** (2000) 4081.
[17] Mayer K. M. and Hafner J. H., *Chem. Rev.*, **111** (2011) 3828.
[18] Zhang J., Xu X., Yuan Y., Yang C. and Yang X., *ACS Appl. Mater. Interfaces*, **3** (2011) 2928.
[19] Chen W. Y., Lan G. Y. and Chang H. T., *Anal. Chem.*, **83** (2011) 9450.
[20] Chen R., Morris H. R. and Whitmore M., *Sens. Actuators B: Chem.*, **186** (2013) 431.
[21] Albery W. J., Cass A. E. G. and Shu Z. X., *Biosens. Bioelectron.*, **5** (1990) 367.
[22] Yang Y., Yang M., Wang H. *et al.*, *Sens. Actuators B: Chem.*, **102** (2004) 162.
[23] Liu L., Chen Zhichun, Yang Shaoming *et al.*, *Sens. Actuators B: Chem.*, **129** (2008) 218.
[24] Shahidi Pour Savizi I., Kariminia H. R., Ghadiri M. and Roosta-Azad R., *Biosens. Bioelectron.*, **35** (2012) 297.
[25] Kariminia H. R., Ghadiri M. and Roosta-Azad R., *Ecotoxicol. Environ. Safety*, **91** (2013) 117.
[26] Strianese M., De Martino F., Pellecchia C., Ruggiero G. and D'Auria S., *Protein Pept. Lett.*, **18** (2011) 282.
[27] Strianese M., Palm G. J., Milione S., Kuhl O., Hinrichs W. and Pellecchia C., *Inorg. Chem.*, **51** (2012) 11220.
[28] Sato F., Yoshihino T., Era M. and Kashiwag H., *Chem. Phys. Lett.*, **341** (2001) 645.
[29] Yoshimura T., Suzuki S., Nakahara A., Iwasaki H., Masuko M. and Matsubara T., *Biochemistry*, **25** (1986) 2436.
[30] Yoshimura T., Fujii S., Kamada H., Yamaguchi K., Suzuki S., Shidara S. and Takakuwa S., *Biochim. Biophys. Acta*, **1292** (1996) 39.
[31] Sandra M. S. and de Oliveira J. F., *J. Dispers. Sci. Technol.*, **23** (2002) 837.
[32] Guillaume S., Christian S., Olivier J. F. and Vera I. S., *Biosens. Bioelectron.*, **42** (2013) 385.
[33] Mattson B., Anderson M. and Mattson S., *Microscale Gas Chemistry Book*, 4th edition (Educational Innovations) 2003.
[34] Gomes I., Santos N. C., Oliveira L. M. A., Quintas A., Eaton P., Pereira E. and Franco R. J., *Phys. Chem. C*, **112** (2008) 16340.
[35] Mie G., *Ann. Phys. (Berlin)*, **330** (1908) 377.
[36] Aden A. L. and Kerker M., *J. Appl. Phys.*, **22** (1951) 1242.
[37] Du H., *Appl. Opt.*, **43** (2004) 1951.
[38] Ovidio P., Pablo P. and Umapada P., *Int. J. Spectrosc.*, **2011** (2011) 583743.
[39] Yang W., *Appl. Opt.*, **42** (2003) 1710.
[40] Yeung C. *et al.*, *Langmuir*, **15** (1999) 6829.
[41] Hirota S., Hayamizu K., Okuno T., Kishi M., Iwasaki H., Kondo T., Hibino T., Takabe T., Kohzuma T. and Yamauchi O., *Biochemistry*, **39** (2000) 6357.